



Modeling total solar irradiance: the data, the models, the questions

S. R. Walton

San Fernando Observatory, Department of Physics and Astronomy, California State University Northridge, 18111 Nordhoff St., Northridge, CA 91330-8268
e-mail: stephen.walton@csun.edu

Abstract. A brief review is given of the modeling of total solar irradiance (TSI) variations as they have been carried out at the San Fernando Observatory over the last few years. The modeling techniques used are described, and recent results of the modeling are summarized, with the goal of showing what may be learned from TSI modeling using ground based observations. I then discuss some very recent results which are part of ongoing investigations: historical reconstruction of TSI using a new technique, and an *ab initio* model of the irradiance variations.

1. Modeling the Total Solar Irradiance

The San Fernando Observatory (SFO) operates two photometric telescopes for obtaining full disk solar images, the Cartesian Full Disk Telescopes 1 and 2 (CFDT1 and CFDT2, respectively). CFDT1 obtains 512 square images with $5'' \times 5''$ pixels and began operation in 1985. Images are taken in three filters: 672.3 nm, 10 nm bandpass; 393.4 nm, 1 nm bandpass (added Spring 1988); and 472.3 nm, 10 nm bandpass (added Spring 1988). CFDT2 takes 1024 square images with $2.5'' \times 2.5''$ pixels and began operation in 1992. It operates in the same three bandpasses as CFDT1 and adds three additional filters: 393.4 nm, 0.3 nm bandpass; 997.0 nm, 10 nm bandpass; and 780.0 nm, 10 nm bandpass (added August 2003 in support of SBI).

When modeling the total solar irradiance (TSI), one generally uses a linear combination of two or more quantities which are taken to represent some portion of TSI variations. SFO observations allow true photometric quantities,

rather than proxies, to be used for this purpose. A generic photometric quantity X can be computed by

$$X = \sum_{\text{feature pixels}} C_i \phi(\mu_i) \quad (1)$$

where C_i is the contrast of the i 'th feature pixel, μ_i its value of μ , and $\phi(\mu)$ is a limb darkening curve normalized so that $\sum \phi(\mu)$ over the hemisphere is one.

We routinely compute several quantities from SFO images:

- D_r is the red deficit computed from red sunspot pixels
- E_r is the red excess computed from red facular pixels
- Σ_r is the red *photometric sum* computed from *all* pixels on the red images
- D_K , E_K , and Σ_K computed similarly from Ca II K images.

The TSI is then modeled using linear regressions of various combinations of these indices.

For the best results, we interpolate TSI measurements to the times of our images.

In Preminger et al. (2002), we showed that an irradiance model of the form

$$S = S_0 + a\Sigma_r + b\Sigma_K \quad (2)$$

matches the observed composite S for all of cycle 22 (June 1988–Sept 1996) with $R = 0.96$ and $\sigma = 0.18 \text{ W m}^{-2}$ (130 ppm). A graph of Σ_r vs. time for cycle 22 is virtually flat, implying that continuum variations make no contribution to the 11-year variation in S . However, Σ_K is strongly correlated with the 11-year variation, indicating that line blanketing changes drive the 11-year change in S . In this view, we divide influences on S by spectrum rather than feature type. Similar results were obtained in observations by Mitchell and Livingston (1991) and the TSI model of Unruh et al. (1999).

1.1. Some Recent Results

White and de Toma (2005) have modeled S using various combinations of parameters. They find that a combination of Σ_r and the Mg ii core/wing ratio give the best fit (as measured by R^2) to the composite TSI for cycle 23, with the resulting model being

$$S = 1365.40 + 19.32 \times \text{Mgii} + 1.188\Sigma_r. \quad (3)$$

For this fit, $R = 0.963$ and the RMS deviation between the fit and the model is 105 ppm. The authors also found that a fit carried out to a any 3-year period in cycle 23 gives essentially the same result, indicating consistency within the cycle and that a relatively short period is all that is required for an adequate model.

White and de Toma (2005) also compared coefficients of fits to other spacecraft measurements of TSI. To the authors' surprise (their word), the fit coefficients' error ellipses were well separated, as shown in Fig. 1.1. This means that the *slopes*, not just the zero points, in the fits differ from one spacecraft to another.

Note that the Nimbus-7 fit is substantially improved by correction for "jumps" in the data zero level computed by Chapman et al. (1996); these jumps are the source of the disagreement

on the change in solar minimum TSI level from 1986 to 1996 (Willson and Mordvinov 2003; Fröhlich and Lean 2004). The fits to SIM are the best we've ever seen: RMS deviation is only 76 ppm! But the time period is still rather short (two years used in this paper)

One of the key questions in the field of solar irradiance modeling is to what extent ground based measurements can aid in interpretation of the spacecraft measurements. The work described here makes it clear that ground based measurements and the models constructed from them can be of great help in interpreting the results from space. Quoting directly from White and de Toma (2005) :“the fitting coefficients can vary substantially from experiment to experiment because of properties of the time series for both TSI and the indices.” The differences in their work are not solar in origin, but are differences between TSI time series when regressed against a common photometric database.

2. Longer Term Irradiance Models

All models of TSI use two (or more) components to model it, such as the Σ_r and Σ_K we describe above, which represent the contribution of sunspots and of bright features such as faculae, respectively. However, measurements of the bright features have only been made relatively recently, so reconstructing TSI on longer timescales requires using the available sunspot data to produce a facular record. In Preminger and Walton (2005), we describe a new technique for modeling the total solar irradiance using the sunspot area record kept at Greenwich Observatory since 1874. Specifically, changes in TSI $\Delta S(t)$ are modeled as a convolution

$$\Delta S(t) = A_S(t) * h(t) \quad (4)$$

where $A_S(t)$ is the sunspot area and $h(t)$ is a *finite impulse response* (FIR) function. In this view, ΔS is the response to the stimulus A_S of a physical system. We assume that the system is linear and time invariant; that is, the convolution integral above represents the response and $h(t)$ is not a function of time. Using

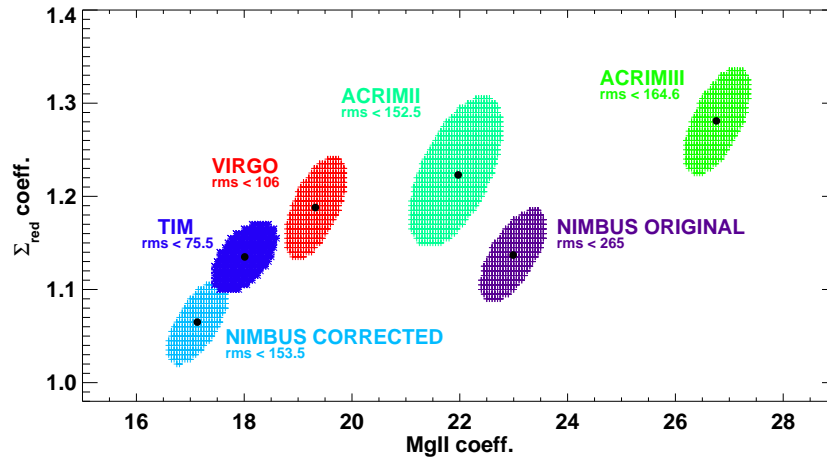


Fig. 1. Error ellipses of the two fit coefficients in Eq. (3) for various solar irradiance spacecraft: ACRIM II, ACRIM III, the VIRGO composite, the Total Irradiance Monitor (TIM) on the SORCE spacecraft, and Nimbus-7 both without and with a correction for two zero level changes in the spacecraft record. Figure reproduced courtesy of G. de Toma and O. R. White.

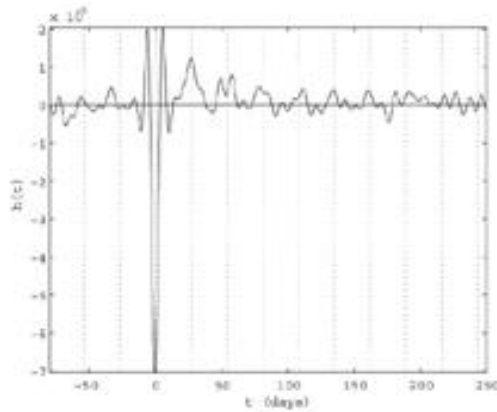


Fig. 2. The portion of the finite impulse response function $h(t)$ defined in equation (4) near $t = 0$.

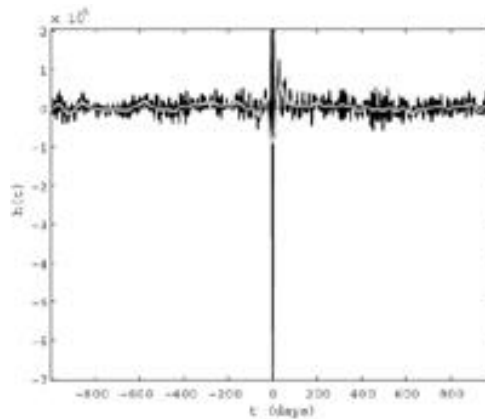


Fig. 3. The entire finite impulse response function $h(t)$ defined in equation (4) (black) and smoothed with a gaussian of FWHM 81 days (gray).

Fourier techniques which are described in detail in Preminger and Walton (2005), we extract $h(t)$ from measurements of $A_s(t)$ and $S(t)$.

In Fig. 2, we show a magnified version of that portion of $h(t)$ near $t = 0$. The sharp negative spike at $t = 0$ represents the downward change in the TSI on the initial disk passage of a sunspot; it is flanked by two peaks which show the net positive change the active region

makes when near the limb. All the succeeding rotational peaks are positive, showing the net positive contribution of the active region on second and subsequent disk appearances. This clearly shows that the average effect of an active region on TSI is positive except for a short period centered on its first central meridian passage.

The entire derived $h(t)$ is shown in Fig. 2. One sees that it basically is at an average of zero for $|t| > 400$ days. Since this time is short compared to the length of the data set used to compute $h(t)$, it is safe to conclude that the FIR is approximately stationary. Fig. 2 also shows that $h(t)$ is positive for $-400 < t < -100$ days. This portion of the FIR represents an increase in the TSI which occurs approximately one year before the rise of the sunspot cycle, a phenomenon which has been documented (Fox 2004). In Preminger and Walton (2005), we tentatively attribute this feature to ephemeral regions, which form an “extended activity cycle” whose rise begins one to two years before the onset of other forms of solar activity Harvey (1993).

Using Eq. (4), we can compute a reconstruction of $\Delta S(t)$ from the convolution integral and $A_s(t)$ once $h(t)$ is known. Since Eq. (4) yields $\Delta S(t)$ to within an additive constant and a possible multiplicative scaling factor, a linear least squares fit to the measured $S(t)$ is required to recover the absolute level and produce the reconstructed TSI record $S_{\text{rec}}(t)$. The least squares fit yields a multiplicative constant indistinguishable from one, indicating that the FIR model yields the overall correct scaling for variations in S .

Fig. 2 shows the result for 1978 to the present; *i.e.*, during the period of time for which $S(t)$ is known from spacecraft measurements. The FIR model accounts for about 80% of the variation in S during the period from 1978 to the present, with the majority of the discrepancy resulting from the breadth of $h(t)$ due to smoothing to reduce noise. This effectively smooths the convolution integral and results in a time series $S_{\text{rec}}(t)$ which does not completely reproduce the short, sharp dips in $S(t)$ which are due to sunspots. Despite some discrepancies during cycle 23, the reconstruction is quite good.

Using the same convolution, we can compute $S_{\text{rec}}(t)$ from 1847 to the present, during the entire time period for which $A_s(t)$ is known. This reconstruction is shown in Fig. 2. Notice the lack of a long term trend in the level of solar minima during this record. Since $h(t)$ is less than 3 years wide, no such trend would

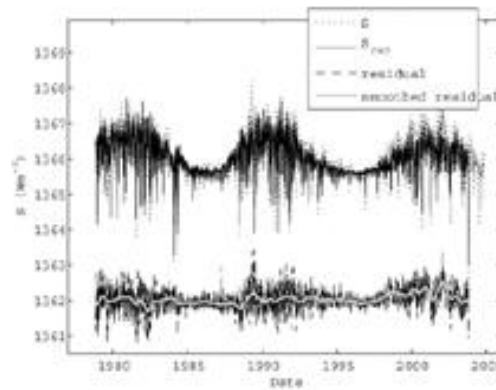


Fig. 4. The top panel shows the total solar irradiance $S(t)$ and $S_{\text{rec}}(t)$ as dashed and solid lines, respectively; $S_{\text{rec}}(t)$ is the TSI as reconstructed from the Finite Impulse Response function computed as in the text, from 1978 to the present. The bottom panel is the residual (black) and smoothed residual (gray).

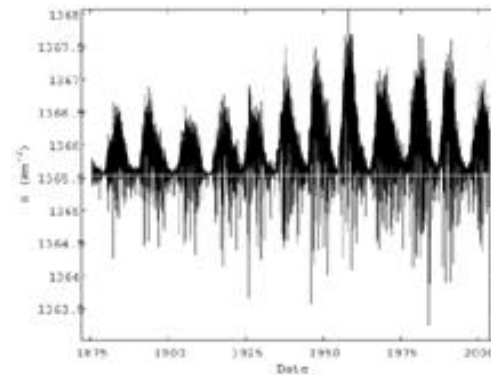


Fig. 5. The total solar irradiance, as reconstructed from the Finite Impulse Response function computed as in the text, from 1874 to the present.

be expected, but $h(t)$ was computed from more than 20 years’ worth of data, using sequences almost two solar cycles wide. Any component of variability in $S(t)$ which was correlated with sunspots on timescales longer than 3 years should, therefore, have been detected when $h(t)$ was computed. We conclude that longer term variations in $S(t)$, if any, are probably not correlated with sunspots, but have a different cause.

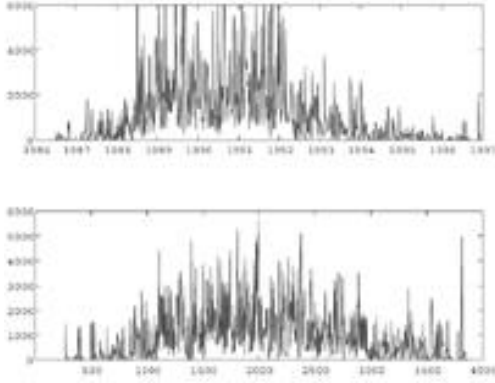


Fig. 6. The true digital sunspot area as measured at SFO (top panel) and the sunspot area from a simulation of the solar cycle with characteristics described in the text (bottom panel).

3. A “Toy” Solar Irradiance Simulation

Most recently, an effort has been made to model the irradiance variations of the Sun. The motivation for this work is twofold: first, to gain some insight into the physical processes which cause the TSI to vary; second, to answer Tom Bogdan’s rhetorical question as to what TSI would look like if we observed the Sun above its pole.

The simulation’s major goals are to match sunspot and facular area time series, and to match as far as possible, auto and cross correlations of facular and sunspot areas. The resulting characteristics of the model are as follows:

1. Active regions of equal area A are generated during each “day” of the simulation.
2. An average of n_{gen} spots per day are generated, with n_{gen} increasing and decreasing smoothly from zero to n_{max} over 4000 days, to emulate the solar cycle.
3. Regions are generated with random longitudes.
4. Regions are generated within the solar activity belts in such a way that the mean latitude decreases smoothly from 25 degrees at the beginning of the cycle to zero at the end, with a ± 5 degree scatter.
5. The sunspot area decays as e^{-t/τ_s} .

6. Decayed sunspot area becomes facular, with a ratio R_{sf} for the conversion of sunspot area into facular area.
7. The facular area decays as e^{-t/τ_f} .

Examination of autocorrelation and cross correlations of sunspot and facular area shows that $\tau_s = 10$ days and $\tau_f = 45$ days are appropriate choices for an approximate description of the sunspot and facular decay. An approximate mimic of cycle 22 results with the following parameters: $n_{\text{max}} = 1/3$, $A = 1500$ microhemispheres, and $R_{fs} = 7$. It should be noted that we are, in effect, generating Ca II K plage in this simulation, hence the large ratio between decayed sunspot area and the resulting facular area.

Fig. 2 shows the results of the simulation for sunspot area and compares the simulation with actual SFO digital sunspot areas for cycle 22. The overall agreement in level is good, but one can see that the actual solar cycle produces, near maximum, numerous regions whose area is larger than the ones we simulate, producing the greater number of large upward spikes in the observed spot area. A comparison of the true and simulated facular area is similar.

In order to model the TSI, we use the Photometric Sunspot Index (PSI) and Photometric Facular Index (PFI) to produce an estimate of D_s and E_f , the deficit and excess due to sunspots and faculae, respectively. The PSI is given by (Foukal 1981)

$$\text{PSI} = \sum C_s A_s \mu (3\mu + 2) / 2 \quad (5)$$

where $C_s = -0.32$ is an assumed constant sunspot contrast, A_s is the true sunspot area, μ is the cosine of the angle between the solar surface normal and the line of sight, and $(3\mu + 2)/2$ is the grey limb darkening curve. The PFI is defined by (Chapman et al. 1996)

$$\text{PFI} = \sum C_f A_f \mu (1/\mu - 1) (3\mu + 2) / 2 \quad (6)$$

where $C_f = 0.036$ and A_f is the true facular area; the factor $(1/\mu + 1)$ is an approximate representation of the facular contrast increase towards the limb.

Once D_s and E_f have been computed, a model change in TSI is computed:

$$\delta S_{\text{mod}} = \text{PSI} + 1.28\text{PFI} \quad (7)$$

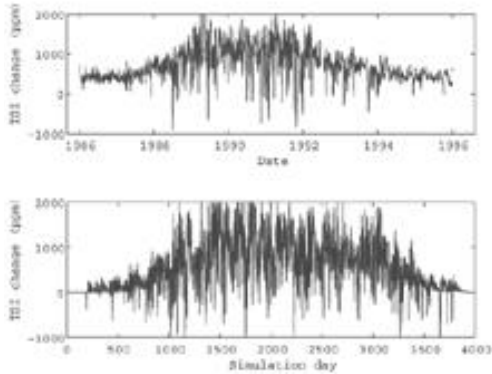


Fig. 7. The relative change in the measured total solar irradiance from cycle 22 (top panel) and that resulting from a simulation of the solar cycle with characteristics described in the text (bottom panel).

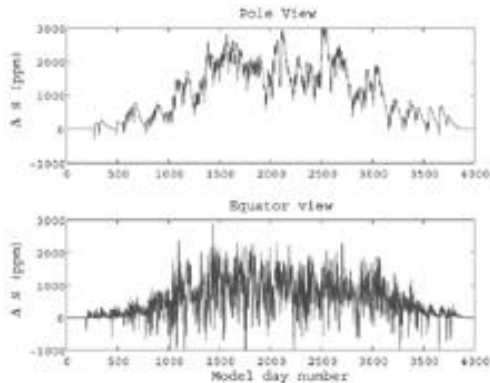


Fig. 8. The relative simulated total solar irradiance as seen from above the simulated Sun's pole (top panel) and from above the equator (bottom panel). Note the much smoother appearance of the pole view. The bottom panel here is the same as that in Fig. 3 but is reproduced here for ease of comparison.

in which the factor of 1.28 is derived from a fit of the measured values of PSI and PFI from SFO images to TSI during solar cycle 22. The results are shown in Fig. 3. The overall increase from solar minimum to maximum has a mean value of about 1000 ppm in both the data and the simulation. However, the simulation clearly produces more large excursions in both directions than the actual data contain. D. Hathaway (2005, private communication) has suggested

this is due to the relatively small number of large active regions in the simulation, and we are presently working on a modified version of the simulation which would generate active regions with a size spectrum similar to that observed on the Sun.

Despite these problems, the appearance of the TSI variation from the pole in the simulation has interesting properties, as shown in Fig. 3. The mean increase is about a factor of two larger in the pole view than in the equator view, but this result is very sensitive to the assumed bolometric facular contrast. Qualitatively, we see that none of the large negative excursions due to sunspots in the equator view are present in the pole view. A polar view of the Sun shows most faculae at values of $\mu < 0.4$; *i.e.*, at latitudes of 25° or less. The simulation shows that the resulting brightness of faculae overwhelms the negative contribution to the TSI of even newborn, large sunspots.

4. A Brief Survey of Other Work

Finally, I survey other recent work on solar irradiance modeling. This is not a comprehensive list, but is rather a selection of results which bear directly on the previous discussions.

Krivova et al. (2003) and Wenzler et al. (2005, 2004) use a spectral synthesis technique to model the TSI from simultaneous magnetic and intensity images from the Michelson Doppler Interferometer on SOHO and from the Kitt Peak Vacuum Telescope, respectively. Their most recent work shows that a model with a single free parameter can reproduce the observed irradiance variations in both solar cycles 22 and 23. These types of spectral irradiance reconstructions have the potential to illuminate portions of the solar spectrum in which the variation takes place.

Fontenla et al. (2004) have investigated spectral irradiance variations in the infrared, using a spectral synthesis technique. They find that the models predict a decrease in the infrared spectral irradiance with increasing solar activity, while the data show an increase. This result is related to uncertainties in the facular

contrast curve in the infrared, and show that some basic questions about the contributions to irradiance variations in different spectral bands remain unanswered.

Using a new instrument, the Solar Bolometric Imager (SBI), Foukal et al. (2004) have carried out the first broadband measurements of facular contrast. They find good agreement between these measurements and a simple computation which uses the continuum contrast of faculae and the Planck curve to compute the bolometric facular contrast. Foukal et al. (2005) use this contrast curve to compute an *ab initio* model of the total solar irradiance, with extremely good results. Presentations by representatives all of these groups are contained in these meeting proceedings, and I commend them to your attention.

Acknowledgements. Research at SFO is supported by California State University Northridge, the National Science Foundation, and NASA. My colleagues Gary Chapman, Angie Cookson, Jan Dobias, and especially Dora Preminger have all made major contributions to this work. My sincere thanks to the Local Organizing Committee for the financial support which enabled me to attend the meeting.

References

- Chapman G. A., Cookson A. M., Dobias J. J. 1996, *J. Geophys. Res.*, 101, 13541
- Fontenla J. M., Harder J., Rottman G., et al. 2004, *ApJ*, 605, L85
- Foukal P. 1981, Sunspots and changes in the global output of the sun, in Cram L., Thomas J. (eds.), *The Physics of Sunspots*. Sacramento Peak Observatory, Sunspot, NM, p. 391
- Foukal P., Bernasconi P., Eaton H., Rust D. 2004, *ApJ*, 611, L57
- Foukal P., Bernasconi P. N., Walton S. R. 2005, *AGU Spring Meeting Abstracts*, B2
- Fox P. 2004, *Geophysical Monograph*, Vol. 141, Pap J. M., Fox P. (eds.), *Solar Variability and Its Effects on Climate*. American Geophysical Union, Washington DC, Ch. *Solar Activity and Irradiance Variations*, 141
- Fröhlich C., Lean J. 2004, *A&A Rev.*, 12, 273
- Harvey K. L. 1993, Ph.D. thesis, University of Utrecht
- Krivova N. A., Solanki S. K., Fligge M., Unruh Y. C. 2003, *A&A*, 399, L1
- Mitchell W. E., Livingston W. C. 1991, *ApJ*, 372, 336
- Preminger D. G., Walton S. R. 2005, *Geophys. Res. Lett.*, 32, L14109
- Preminger D. G., Walton S. R., Chapman G. A. 2002, *Journal of Geophysical Research (Space Physics)*, 107(A11), 1354
- Unruh Y. C., Solanki S. K., Fligge M. 1999, *A&A*, 345, 635
- Wenzler T., Solanki S. K., Krivova N. A. 2005, *A&A*, 432, 1057
- Wenzler T., Solanki S. K., Krivova N. A., Fluri D. M. 2004, *A&A*, 427, 1031
- White O. R., de Toma G. 2005, *AGU Spring Meeting Abstracts*, B6
- Willson R. C., Mordvinov A. V. 2003, *Geophys. Res. Lett.*, 30(5), 1199